Journal of Alloys and Compounds 509 (2011) 5777–5782

Contents lists available at ScienceDirect

Journal of Alloys and Compounds

journal homepage: www.elsevier.com/locate/jallcom

# Synthesis and photoluminescence properties of color-tunable $BaLa_2WO_7:Eu^{3+}$ phosphor

Shao-An Yan [a], Yee-Shin Chang [b], Weng-Sing Hwang [a,*], Yen-Hwei Chang [a], Masahiro Yoshimura [a], Chii-Shyang Hwang [a]

[a] Department of Materials Science and Engineering, National Cheng Kung University, Tainan 701, Taiwan
[b] Department of Electronic Engineering, National Formosa University, Huwei, Yunlin 632, Taiwan

ARTICLE INFO

*Article history:*
Received 20 October 2010
Received in revised form 18 February 2011
Accepted 19 February 2011
Available online 24 February 2011

*Keywords:*
Phosphor
$BaLa_2WO_7$
Europium doping
Color-tunable

ABSTRACT

Color-tunable phosphors $BaLa_{2-x}Eu_xWO_7$ were synthesized via a solid-state reaction. The absorption, excitation, emission and decay curves were obtained to study the luminescence properties. The experimental results indicate that $BaLa_{2-x}Eu_xWO_7$ phosphors have two regions in the excitation spectra: one is assigned to the charge-transfer state (CTS) band at about 338 nm, and the other is assigned to the intra-4f transitions at 360–600 nm. The emission spectra of $BaLa_{2-x}Eu_xWO_7$ phosphors excited at 395 nm exhibit a series of sharp peaks, which are attributed to the $^5D_0 \rightarrow {}^7F_J$ ($J = 0, 1, 2, 3, 4$) transitions. Luminescence from higher excited states, such as $^5D_1$, $^5D_2$, and $^5D_3$, were also observed at low $Eu^{3+}$ concentration. The optimal emission intensity of $^5D_0 \rightarrow {}^7F_2$ red emission is at $x = 0.4$ ($BaLa_{1.6}Eu_{0.4}WO_7$). The chromaticity coordinates of $BaLa_{2-x}Eu_xWO_7$ phosphors vary with $Eu^{3+}$ content from white, orange-red, to red, making it a candidate for a white-light-emitting phosphor in UV-LEDs.



## 1. Introduction

White-light-emitting diodes (WLEDs) are potential replacements for incandescent light sources. The most common WLEDs use a 450–470 nm blue-light-emitting diode that excites a yellow-light-emitting yttrium aluminum garnet (YAG:$Ce^{3+}$) phosphor dispersed in an epoxy resin on a blue LED chip [1–3]. However, a single yellow phosphor cannot achieve low color temperatures, leading to a low color rendering index [4]. To overcome these problems, UV-LEDs with triple-wavelength red–green–blue phosphors have been developed [5–7]. More recently, single-phase white-light-emitting phosphors have received a lot of attention for application in WLEDs [8–11].

For near-UV and blue LED applications, $Eu^{3+}$-doped oxide phosphors exhibit a high quantum efficiency and high photostability. A fluorescent light source comprising a red line emitter emitting at 610–616 nm is the best compromise between luminance and color rendering. For $Eu^{3+}$-doped oxide phosphors, the most intense emission lines are located in this spectral range. The main strategy for further enhancing the luminescence properties of $Eu^{3+}$-doped oxide phosphors is finding suitable host materials, in which the $Eu^{3+}$ ions can occupy a lattice site with low symmetry and which have strong covalent interaction between the activator and the surrounding anions [12–15]. To achieve this, $Eu^{3+}$ ions can be doped into highly covalent oxide lattices, such as molybdates, indates, and tungstates, where the activator ions can be incorporated onto lattice sites such as $Ga^{3+}$, $Y^{3+}$, and $La^{3+}$ ions [12]. In particular, a proper host material doped with $Eu^{3+}$ can generate red emission from the $^5D_0$ level and green and blue emissions from higher $^5D$ levels such as $^5D_1$, $^5D_2$, and $^5D_3$ of $Eu^{3+}$, to obtain single-phase white-light-emitting phosphors [8–11].

$BaLa_2WO_7$ has been reported as a red-emitting phosphor [16]. In the present study, $BaLa_2WO_7$ was chosen as the host material. $BaLa_2WO_7$ has a monoclinic structure with space group $P2_1/b$, and lattice parameters $a = 8.857$ (Å), $b = 12.872$ (Å), $c = 5.830$ (Å), and $\gamma = 105.16^\circ$ [17]. The cations in $BaLa_2WO_7$ are arranged in positions corresponding to a face-centered cubic (fcc) lattice related to the fluorite lattice. $BaO_{11}$, $LaO_{11}$, and $LaO_9$ polyhedra exist in this structure, and the $WO_6$ octahedral environment of the tungsten was confirmed by Balashov et al. [18]. In the present study, $Eu^{3+}$-activated $BaLa_2WO_7$ was synthesized using a solid-state reaction and its photoluminescence properties were studied. A high-color-purity red phosphor and single-phase white-emitting phosphors of $BaLa_2WO_7:Eu^{3+}$ for near-UV light excitation are demonstrated.

## 2. Experimental procedures

### 2.1. Synthesis and characterization

Specimens of $Eu^{3+}$-ion-doped $BaLa_2WO_7$ were synthesized via a solid-state reaction. The raw materials were $BaCO_3$ (Alfa Aesar), $La_2O_3$ (SHOWA), $WO_3$ (Alfa Aesar),

* Corresponding author. Tel.: +886 62757575x62928; fax: +886 62344393.
*E-mail address:* wshwang@mail.ncku.edu.tw (W.-S. Hwang).

0925-8388/$ – see front matter © 2011 Elsevier B.V. All rights reserved.
doi:10.1016/j.jallcom.2011.02.103

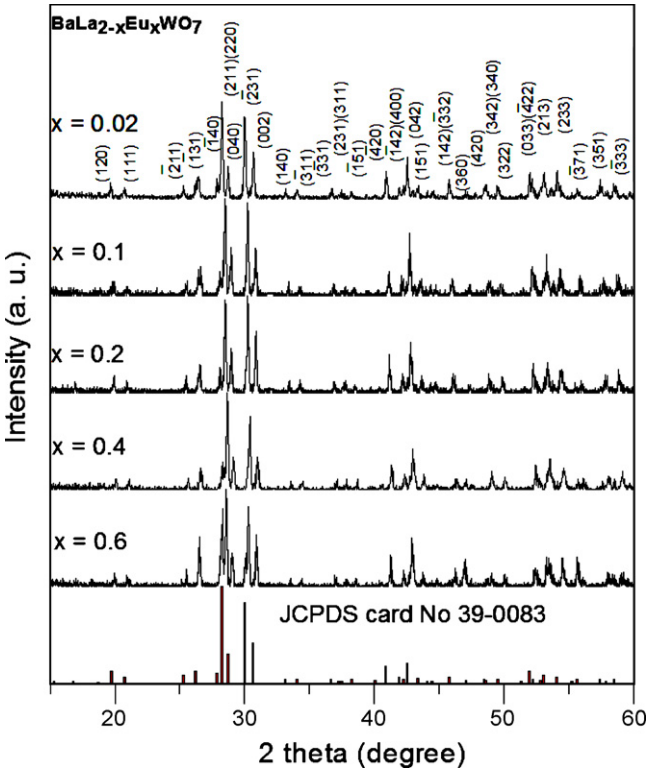


**Fig. 1.** The X-ray diffraction patterns of $BaLa_{2-x}Eu_xWO_7$ ($x$ = 0–0.6) prepared at 1350 °C for 8 h.

and $Eu_2O_3$ (Alfa Aesar) with purities of 99.99%. The materials were weighed in a stoichiometric ratio and ground in a mechanically activated high-energy vibro mill for 20 min with zirconia balls in a polyethylene jar. After grinding, the mixtures were fired at 1350 °C for 8 h in air. The X-ray diffraction of the samples was examined on a Rigaku Dmax diffractometer using Cu Kα radiation (λ = 0.15406 nm) with a source power of 30 kV and a current of 20 mA to identify the phase of the product. The excitation and emission spectra of these phosphors were measured with a Hitachi F-4500 fluorescence spectrophotometer using a Xe lamp as the excitation source at room temperature.

### 2.2. Vibrating mill method

The vibrating mill method was employed in this experiment. The reactant powder mixture and the milling balls are contained in a polyethylene jar, which is swung back and forth horizontally at the end of an arm (about 15 times per second). The polyethylene jar also wobbles sideways to make the motion of the balls more random. The main milling action comes from the powder being caught between an impacting ball and the end of the polyethylene jar. Compression and shear forces between colliding balls also contribute. The vibrating ball milling method can produce unique and metastable materials via a self-sustaining reaction of highly exothermic powder mixtures. The method comprises four processes: (1) material destruction; (2) formation of a new surface; (3) fine grinding; and (4) transformation into a new material with a completely different structure [19].

The vibrating mill method is used to modify the properties of materials, enhance the reactivity of materials, produce advanced materials, and to separate composite materials into their constituents. When materials are subjected to intensive grinding, their structure and microstructure characteristic greatly change. These structural changes determine the reactivity of materials and play an important role in subsequent processes. The vibrating ball milling method can decrease the decomposition temperature, reduce reagent consumption, and improve the recovery of valuable material components [19].

## 3. Results and discussion

Fig. 1 shows the X-ray diffraction patterns of synthesized $BaLa_{2-x}Eu_xWO_7$ for $x$ = 0–0.6. All the diffraction peaks are in agreement with the JCPDS card (No. 39-0083); no impurity phases were detected. The results reveal that the $La^{3+}$ ions were fully substituted by the $Eu^{3+}$ ions. An unidentified phase appeared when the $Eu^{3+}$ concentration was increased to $x$ = 0.8. The critical concentration for

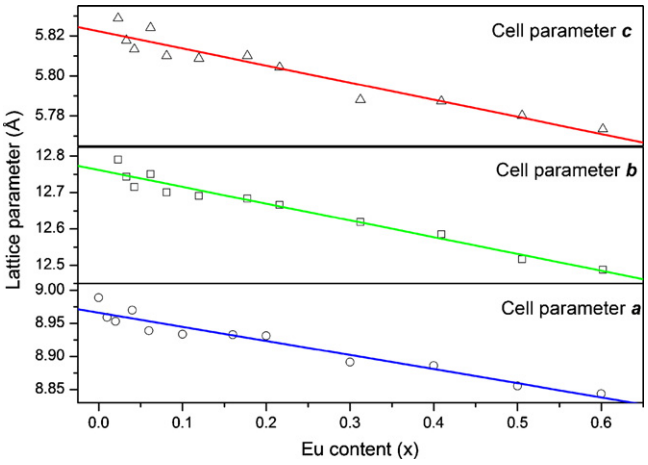


**Fig. 2.** The variations of the monoclinic lattice parameters $a$, $b$ and $c$ axis with the $Eu^{3+}$ content in the $BaLa_{2-x}Eu_xWO_7$ ($x$ = 0.01–0.6) (in Å).

the substitution of $La^{3+}$ ions by $Eu^{3+}$ ions is thus between $x$ = 0.6 and $x$ = 0.8. Fig. 2 shows the lattice parameters for the full substitution of $La^{3+}$ ions by $Eu^{3+}$ ions in $BaLa_{2-x}Eu_xWO_7$ ($x$ = 0–0.6) calculated from the XRD data. The crystal structure gradually shrank along the $a$, $b$, and $c$ axes with increasing $Eu^{3+}$ concentration. A linear relationship was found between the lattice parameters of the monoclinic structure and the concentration of $Eu^{3+}$ ions. The difference in the ionic radius between $La^{3+}$ ions ($r$ = 1.216 Å) and $Eu^{3+}$ ions ($r$ = 1.120 Å) resulted in a decrease of the lattice parameters [20] of the solid solution when $x$ = 0–0.6.

The UV–vis optical absorption spectra of $BaLa_2WO_7$ and $BaLa_{1.6}Eu_{0.4}WO_7$ are shown in Fig. 3. The host absorption of $BaLa_2WO_7$ was detected at 200–230 nm. The broad absorption band from 280 to 360 nm can be assigned to the charge-transfer state (CTS) from oxygen to tungsten ($O^{2-}$–$W^{6+}$) according to the data for $AgGd_{0.95}Eu_{0.05}(WO_4)_{2-x}(MoO_4)_x$ [21]. After $Eu^{3+}$ ions were added to $BaLa_2WO_7$, the $BaLa_{1.6}Eu_{0.4}WO_7$ sample exhibited a definite CTS from oxygen to europium ($O^{2-}$–$Eu^{3+}$) between 230 and 260 nm. In addition, several sharp peaks from 360 to 700 nm appeared for the $BaLa_{1.6}Eu_{0.4}WO_7$ sample, which are associated with typical intra-4$f$ forbidden transitions of $Eu^{3+}$ ions.

The excitation spectra of all $BaLa_{2-x}Eu_xWO_7$ samples were similar. Fig. 4 shows the excitation spectrum of $BaLa_{1.6}Eu_{0.4}WO_7$ monitored at 616 nm. The broad band at about 338 nm can be

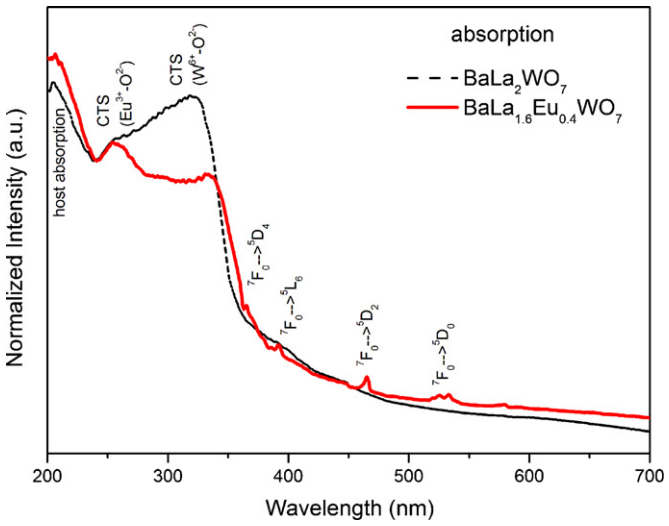


**Fig. 3.** The UV–vis optical absorption spectra of $BaLa_2WO_7$ and $BaLa_{1.6}Eu_{0.4}WO_7$.

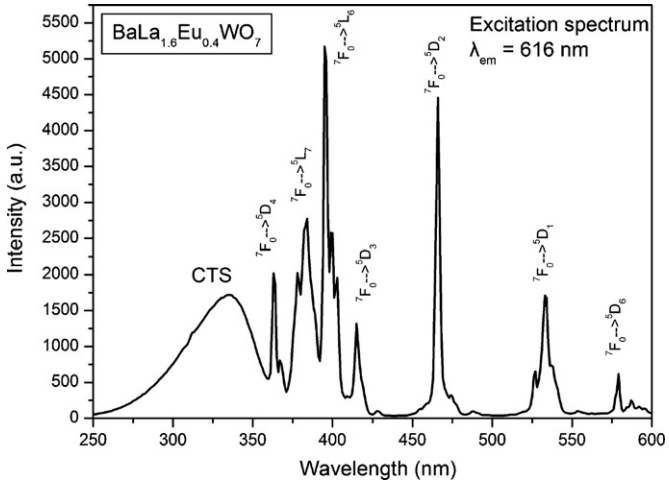


**Fig. 4.** Photoluminescence excitation spectra of solid-state reaction synthesized $BaLa_{1.6}Eu_{0.4}WO_7$ powders prepared at 1350 °C for 8 h.

assigned to the CTS from oxygen to tungsten (ligand-to-metal charge-transfer, LMCT) of the host lattice. In the excitation spectra, the host absorption band and the charge-transfer band of $Eu^{3+}$–$O^{2-}$ were not clearly detected, which might be due to a possible overlap of the CT band with that of the tungstate group found in $AgGd_{0.95}Eu_{0.05}(WO_4)_{2-x}(MoO_4)_x$ [19]. According to the data reported for other tungstate phosphors [22–25], the CTS band of the $WO_6$ group is located between 250 and 360 nm. However, the CTS band of the oxygen 2*p* orbital to the empty 4*f* orbital of $Eu^{3+}$ is weak and immersed in the CTS band from the $WO_6$ group [22–25]. The sharp peaks between 360 and 600 nm can be attributed to the intra-4*f* forbidden transitions of $Eu^{3+}$, which is consistent with the UV–vis optical absorption spectrum of $BaLa_{1.6}Eu_{0.4}WO_7$. The dominant excitation peak lines at 395 nm and 466 nm are attributed to the $^7F_0 \rightarrow {}^5L_6$ and $^7F_0 \rightarrow {}^5D_2$ transitions, respectively. These results are in agreement with those found in previous reports [21–23], so it can be concluded that the $BaLa_{2-x}Eu_xWO_7$ phosphors can be excited by blue or near-UV light.

The excitation spectra of $BaLa_{1.98}Eu_{0.02}WO_7$ phosphor in the UV region of 200–400 nm monitored at the emission wavelengths of 415 nm for the $^5D_3 \rightarrow {}^7F_1$ transition (Fig. 5a), 469 nm for the $^5D_2 \rightarrow {}^7F_1$ transition (Fig. 5b), 533 nm for the $^5D_1 \rightarrow {}^7F_1$ transition (Fig. 5c), and 616 nm for the $^5D_0 \rightarrow {}^7F_2$ transition (Fig. 5d) are shown in Fig. 5. The broadband centered at 338 nm should be the CTS [21] and the sharp peaks from 360 to 400 nm can be attributed to the intra-4*f* forbidden transition of $Eu^{3+}$ as mentioned above. Fig. 5 also indicates that lower energy states, such as the $^5D_{1,0}$ transition, have a lower intensity of *f*–*f* transition to CTS ratio (*f*–*f* transition/CTS) than those of higher energy states, such as the $^5D_{3,2}$ transition. Similar results were reported in a previous study [22]. This is due to direct energy transfer from CTS to the $^5D_{1,0}$ energy states, which allows the CTS band to feed directly to the lower energy states of $^5D_{1,0}$. In contrast to the CTS band, 4*f* electrons are well shielded from the surroundings by filled 5*s* and 5*p* orbitals [26–28], so the influence of the energy transfer for *f*–*f* transition is too weak to be considered. Therefore, the $^5D_{1,0}$ state transition is more effective than the $^5D_{3,2}$ transition under CTS excitation [29].

Fig. 6 shows the emission spectra of $BaLa_{1.98}Eu_{0.02}WO_7$ phosphor for various excitation wavelengths. It should be noted that these results show completely different radiation ratios between $^5D_{1,0}$ and $^5D_{3,2}$ transitions under excitation wavelengths of 338 nm and 395 nm. The intensities of the $^5D_{3,2}$ transition emission line are lower than those of other $^5D_{1,0}$ emission lines under the excitation wavelength of 338 nm; the opposite is true for the excitation wavelength of 395 nm. This result can be explained by the direct energy transfer from the CTS band described above.

The emission spectra of $BaLa_{2-x}Eu_xWO_7$ phosphors with various $Eu^{3+}$ concentrations under an excitation wavelength of 395 nm are shown in Fig. 7. The characteristic peaks of $Eu^{3+}$ ion intra-$4f^6$ transitions from excited states to lower levels are $^5D_0$ (red emission) $\rightarrow {}^7F_J$ ($J$ = 0, 1, 2), $^5D_1$ (green emission) $\rightarrow {}^7F_J$ ($J$ = 0, 1, 2, 3), $^5D_2$ (blue–green emission) $\rightarrow {}^7F_J$ ($J$ = 0, 1, 2, 3), and $^5D_3$ (blue emission) $\rightarrow {}^7F_J$ ($J$ = 1, 2, 3). The emission spectra show com-

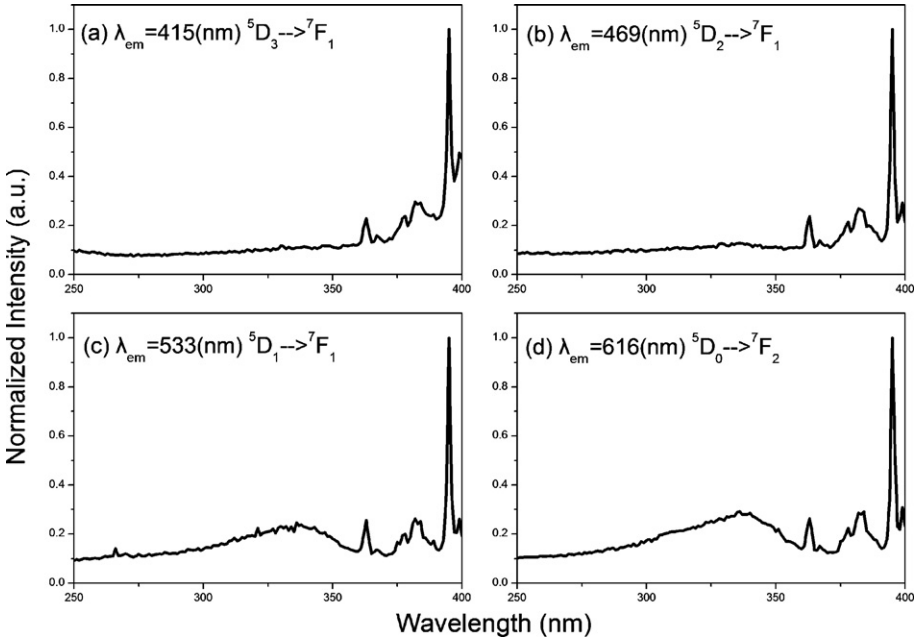


**Fig. 5.** Photoluminescence excitation spectra of $BaLa_{1.98}Eu_{0.02}WO_7$ prepared at 1350 °C for 8 h monitored at emission wavelength of (a) 415 nm, (b) 469 nm, (c) 533 nm, and (d) 616 nm.

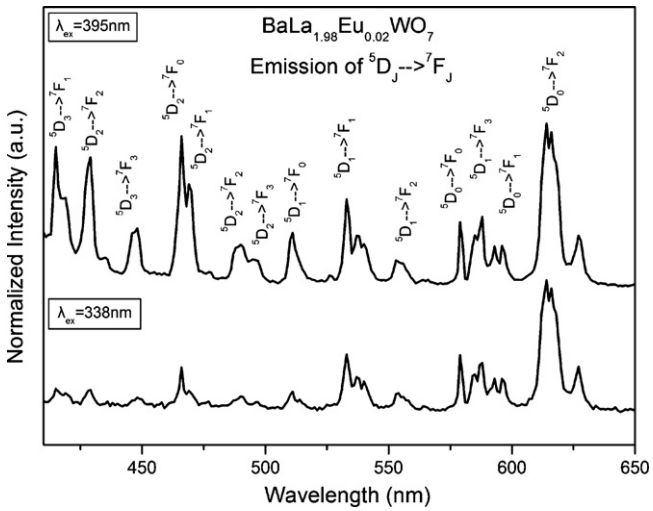


**Fig. 6.** Photoluminescence emission spectra of $BaLa_{1.98}Eu_{0.02}WO_7$ prepared at 1350 °C for 8 h under excitations of 395 and 338 nm.

pletely different ratios between the $^5D_{1,2,3}$ blue–green emission and the $^5D_0$ red emission for low and high $Eu^{3+}$ concentrations. The emission intensity from $^5D_0 \rightarrow {}^7F_J$ transitions increases with increasing $Eu^{3+}$ concentration, whereas the intensity of the emission from $^5D_{1,2,3}$ gradually decreases. It can thus be concluded that the color tunability is due to concentration quenching via the cross-relaxation mechanism [30]. In this non-radiative process, excitation energy from decaying ions leads to a higher excited state ($^5D_{1,2,3}$) of $Eu^{3+}$, which promotes a neighboring ion from the ground state to a metastable state level, such as $^5D_1(Eu_1) + {}^7F_0(Eu_2) \rightarrow {}^5D_0(Eu_1) + {}^7F_3(Eu_2)$ [26]. Consequently, the lower level emission becomes dominant when the $Eu^{3+}$ concentration is sufficiently high and the higher level emission can be easily quenched via cross-relaxation. The dominant emission peaks at 596 and 616 nm are assigned to the $^5D_0 \rightarrow {}^7F_1$ magnetic dipole transition and the $^5D_0 \rightarrow {}^7F_2$ electric-dipole transition of $Eu^{3+}$, respectively. The electric dipole transition $^5D_0 \rightarrow {}^7F_2$ with $\Delta J = 2$ is hypersensitive and strongly influenced by ligand ions in the crystal lattice [31]. However, the $^5D_0 \rightarrow {}^7F_1$ is the magnetic dipole transition, which hardly varies with the crystal field strength according to the Judd-Ofelt theory [32]. The $(^5D_0 \rightarrow {}^7F_2)/(^5D_0 \rightarrow {}^7F_1)$ emission ratio, called the asymmetry ratio, can be used as an index to measure the degree of distortion from the inversion symmetry of the local environment around the $Eu^{3+}$ ions in the host lattice [33–36]. When $Eu^{3+}$ ions occupy a low-symmetry site, the $^5D_0 \rightarrow {}^7F_2$ electric-dipole transition often dominates the emission spectrum. In the $BaLa_{2-x}Eu_xWO_7$ phosphors, the emission intensity of the $^5D_0 \rightarrow {}^7F_2$ transition is more sensitive than that of the $^5D_0 \rightarrow {}^7F_1$ transition, which indicates that $Eu^{3+}$ ions have no inversion center. Fig. 8 shows the dependence of the $(^5D_0 \rightarrow {}^7F_2)/(^5D_0 \rightarrow {}^7F_1)$ asymmetry ratio on $Eu^{3+}$ concentration in $BaLa_{2-x}Eu_xWO_7$ phosphors under an excitation wavelength of 395 nm. Since the asymmetry ratio increased with increasing $Eu^{3+}$ concentration, it can be concluded that the local structural symmetry around $Eu^{3+}$ significantly changed as $Eu^{3+}$ became incorporated into $BaLa_{2-x}Eu_xWO_7$.

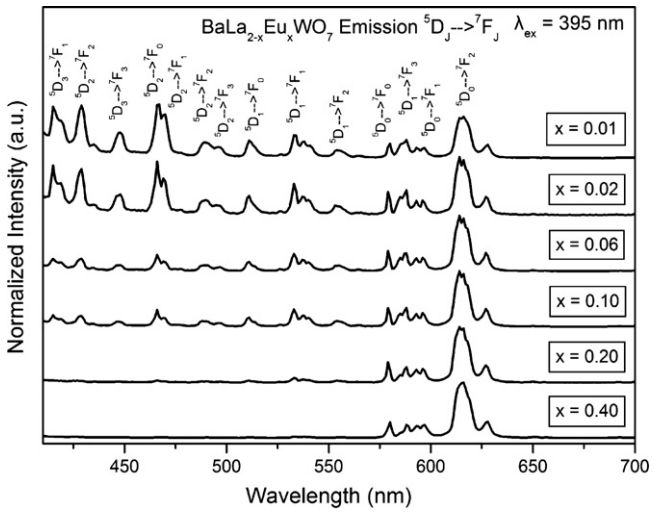


**Fig. 7.** Photoluminescence emission spectra of $BaLa_{2-x}Eu_xWO_7$ doped with various amounts of $Eu^{3+}$ prepared at 1350 °C for 8 h.

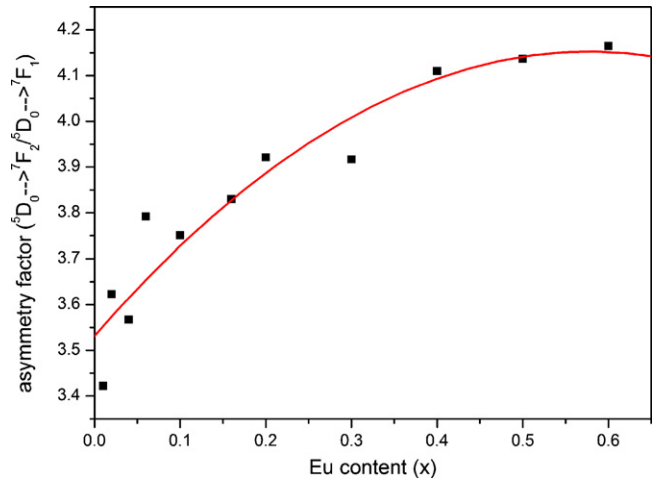


**Fig. 8.** The dependence of asymmetry ratio on $Eu^{3+}$ content in $BaLa_{2-x}Eu_xWO_7$ under excitation at 395 nm.

The relative emission intensity and decay time behavior of the $^5D_0 \rightarrow {}^7F_2$ transition dependence of the $Eu^{3+}$ concentration under excitation at 395 nm are shown in Fig. 9. The decay time of $BaLa_{2-x}Eu_xWO_7$ samples does not change significantly with increasing $Eu^{3+}$ concentration for $x < 0.6$. This means that the emission intensity increased with $Eu^{3+}$ concentration until $x = 0.4$, and then began to decrease with a further increase in the $Eu^{3+}$ content. This phenomenon can be regarded as concentration quenching, which is due to an increase in the number of non-radiative decay channels that leads to energy migration to crystalline defects or trace ions (energy transfer from one activator to another) until the energy sink in the lattice is reached [37]. However, the present

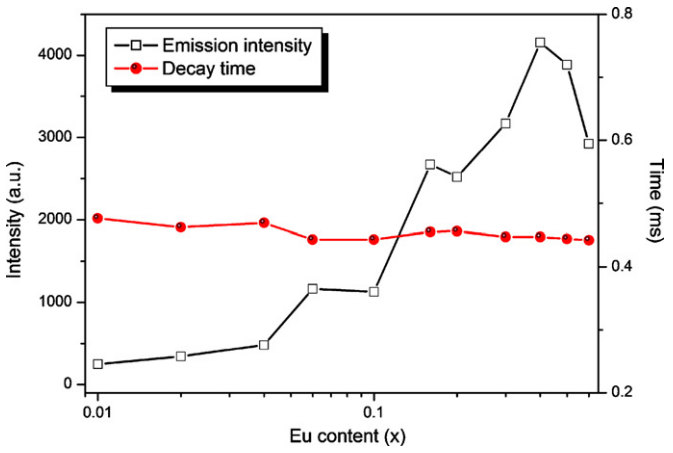


**Fig. 9.** The variation of emission intensity and decay time of the $^5D_0 \rightarrow {}^7F_2$ transition with $Eu^{3+}$ concentration in $BaLa_{2-x}Eu_xWO_7$ under excitation at 395 nm. The signals were detected at 616 nm.

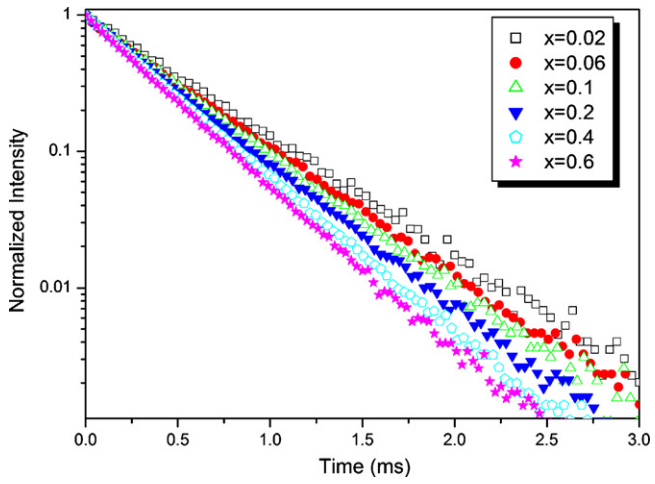


**Fig. 10.** Normalized decay curves of $^5D_0 \rightarrow {}^7F_2$ transition for $Eu^{3+}$ in $BaLa_{2-x}Eu_xWO_7$.

phosphors do not exhibit similar effects. Fig. 10 shows the effect of $Eu^{3+}$ content on the $^5D_0 \rightarrow {}^7F_2$ transition decay curves under excitation at 395 nm. All decay curves were fitted by the single exponential decay $I = I_0 \exp(-t/\tau)$, where $I_0$ and $I$ are the luminescence intensities at time 0 and $t$, respectively, and $\tau$ is the radiative decay time. The results indicate that the $Eu^{3+}$ environment is unique, in accordance with the crystal structure, and that only one local $Eu^{3+}$ environment exists [37–40]. It is thus suggested that the $Eu^{3+}$ ions were shielded by La and W polyhedrals in the $BaLa_2WO_7$ structure, which caused a weak energy transfer between $Eu^{3+}$ pairs. All of these curves can be well fitted by monoexponential decay regardless of $Eu^{3+}$ concentration. This is a unique characteristic of the present phosphors.

The Commission Internationale de l'Eclairage (CIE) chromaticity coordinates with various color tones for $BaLa_{2-x}Eu_xWO_7$ phosphors excited at 395 nm are illustrated in Fig. 11. With increasing $Eu^{3+}$ ion concentration, the color tone changes from white, through red-orange, and finally to red with a CIE chromaticity of (0.62, 0.34), which is close to the standard red chromaticity (0.67, 0.33) for the National Television Standard Committee (NTSC) system. In particular, $BaLa_{1.98}Eu_{0.02}WO_7$ phosphors show white-light emission with CIE coordinates (0.33, 0.26). This result indicates that the emission color of $BaLa_{2-x}Eu_xWO_7$ phosphors can be tuned using the $Eu^{3+}$ ion concentration without doping other color centers in a single-phase host lattice. The proposed host material is thus suitable for use as a near-UV to blue LED converted phosphor.

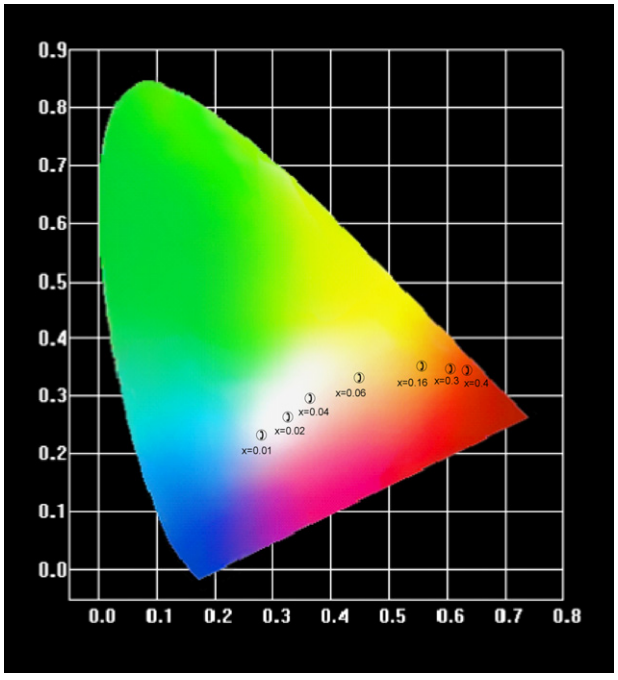


**Fig. 11.** CIE color coordinate diagram of $BaLa_{2-x}Eu_xWO_7$ phosphors. (For interpretation of the references to color in this figure legend, the reader is referred to the web version of the article.)

## 4. Conclusions

Color-tunable $BaLa_{2-x}Eu_xWO_7$ phosphors were synthesized via a solid-state reaction. The two most intense excitation peak lines, observed at 395 and 466 nm, are attributed to the $^7F_0 \rightarrow {}^5L_6$ and $^7F_0 \rightarrow {}^5D_2$ transitions, respectively, which shows that the $BaLa_{2-x}Eu_xWO_7$ phosphors can be excited by blue or UV-LED chips. $BaLa_{1.98}Eu_{0.02}WO_7$ phosphors show white-light emission with a CIE chromaticity of (0.33, 0.26). With increasing $Eu^{3+}$ ion concentration, the color tone changes from white, through red-orange, and finally to red with a CIE chromaticity of (0.62, 0.34). Thus, the emission color of $BaLa_{2-x}Eu_xWO_7$ phosphors can be tuned using $Eu^{3+}$ ion concentration without doping other color centers in a single-phase host lattice. The optimal emission intensity of the $^5D_0 \rightarrow {}^7F_2$ red emission is at $x = 0.4$ ($BaLa_{1.6}Eu_{0.4}WO_7$). The results show that $BaLa_{2-x}Eu_xWO_7$ can potential be a red-emitting phosphor used in both near-UV and blue LEDs.

## Acknowledgement

The authors would like to thank the Bureau of Energy, Ministry of Economic Affairs (99-D0204-2) in Taiwan for financially supporting this research.

## References

[1] Y. Shimizu, K. Sakano, Y. Noguchi, T. Moriguchi, U.S. Pat. 5998925 (1998).
[2] Y. Sang, H. Liu, Y. Lv, J. Wang, T. Chen, D. Liu, X. Zhang, H. Qin, X. Wang, R.I. Bpughton, J. Alloys Compd. 490 (2010) 459–462.
[3] R. Praveena, L. Shi, K.H. Jang, V. Venkatramu, C.K. Jayasankar, H.J. Seo, J. Alloys Compd. 509 (2011) 859–863.
[4] K. Toda, Y. Kawakami, S.I. Kousaka, Y. Ito, A. Komeno, K. Uematsu, M. Sato, IEICE Trans. Electron. E89-C (2006) 1406.
[5] T. Nishida, T. Ban, N. Kobayashi, Appl. Phys. Lett. 82 (2003) 3817.
[6] X. Li, L. Guan, X. Li, J. Wen, Z. Yang, Powder Technol. 200 (2010) 12–15.
[7] Z. Rui, W. Xiang, J. Alloys Compd. 509 (2011) 1197–1200.
[8] X. Liu, C. Lin, J. Lin, Appl. Phys. Lett. 90 (2007) 081904.
[9] T. Hayakawa, A. Hiramitsu, M. Nogami, Appl. Phys. Lett. 82 (2003) 2975.
[10] C.K. Chang, T.M. Chen, Appl. Phys. Lett. 91 (2007) 081902.
[11] Y.C. Liao, C.H. Lin, S.L. Wang, J. Am. Chem. Soc. 127 (2005) 9986.
[12] D. Uhlich, J. Plewa, T. Justel, J. Lumin. 128 (2008) 1649–1654.
[13] X. He, M. Guan, N. Lian, J. Sun, T. Shan, J. Alloys Compd. 492 (2010) 452–455.
[14] X. Wang, S. Zhao, Y. Zhang, G. Sheng, J. Rare Earth 28 (2010) 222.
[15] X. Zhang, H.J. Seo, J. Alloys Compd. 509 (2011) 2007–2010.
[16] C.S. Park, B.Y. Jung, H.K. Moon, J. Korean Phys. Soc. 57 (1) (2010) 169–172.
[17] L.M. Kovba, L.N. Lykova, V.L. Balashov, Russ. J. Inorg. Chem. (Engl. Transl.) 30 (2) (1985) 311.
[18] L.M. Kovba, L.N. Lykova, V.L. Balashov, Russ. J. Inorg. Chem. (Engl. Transl.) 30 (8) (1985) 1210–1212.
[19] K. Tkacova, Elsevier, Amsterdam, 1989.
[20] M.J.J. Lammers, H. Donker, G. Blasse, Mater. Chem. Phys. 13 (1985) 527.
[21] V. Sivakumar, U.V. Varadaraju, J. Electrochem. Soc. 152 (2005) H168.
[22] C.H. Chiu, C.H. Liu, S.B. Huang, T.M. Chen, J. Electrochem. Soc. 155 (3) (2008) J71–J78.
[23] F.N. Shi, J. Meng, Y.F. Ren, J. Solid State Chem. 121 (1996) 236.
[24] F.N. Shi, J. Meng, Y.F. Ren, J. Phys. Chem. Solids 59 (1997) 105.
[25] S. Ye, C.H. Wang, X.P. Jing, J. Electrochem. Soc. 155 (6) (2008) J148–J151.
[26] G. Blasse, B.C. Grabmayie, Luminescence Materials, Springer, Berlin, 1994, pp. 75, 100–101 (Chapters 4 and 5).
[27] Q. Li, J. Huang, D. Chen, J. Alloys Compd. 509 (2011) 1007–1010.
[28] X.Y. Chen, C. Ma, S.P. Bao, H.Y. Zhang, J. Alloys Compd. 497 (2010) 354–359.
[29] J. Alarcon, G. Blasse, J. Phys. Chem. Solids 53 (5) (1992) 667–680.
[30] A.H. Kitai, Solid State Luminescence, Chapman & Hall, U.K., 1993, p. 39.
[31] C.H. Liang, Y.C. Chang, Y.S. Chang, Appl. Phys. Lett. 93 (2008) 211902.

[32] S. Shionoya, W.M. Yen, Phosphor Handbook, CRC Press, 1999 (Chapter 2, p. 88 and Chapter 5, p.179, 190).
[33] C.H. Liang, Y.C. Chang, Y.S. Chang, J. Electrochem. Soc. 156 (10) (2009) J303–J307.
[34] B.S. Tsai, Y.H. Chang, Y.C. Chen, Electrochem. Solid-State Lett. 8 (7) (2005) H55.
[35] B. Yan, F. Lei, J. Alloys Compd. 507 (2010) 460–464.
[36] Q. Lu, J. Li, J. Alloys Compd. 33 (2011) 381–384.
[37] Y.C. Li, Y.H. Chang, Y.F. Lin, Y.S. Chang, Y.J. Lin, Electrochem. Solid-State Lett. 9 (2006) H74.
[38] A.A. Kaminskii, B.V. Mill, A.V. Butashin, E.L. Belokoneva, K. Kurbanov, Phys. Stat. Sol. (a) 103 (1987) 575.
[39] O. Jarchow, K.-H. Klaska, H. Schenk, Naturwiss 68 (1981) 475.
[40] O. Jarchow, K.-H. Klaska, H. Schenk-Strauss, Z. Kristallogr, Naturwiss 172 (1985) 159.